Monte Carlo study of asymmetric 2D XY model

Christian Holm [a], Wolfhard Janke [b,c,*], Tetsuo Matsui [d], Kazuhiko Sakakibara [e]

[a] *Max-Planck-Institut für Polymerforschung, Postfach 3148, 55021 Mainz, Germany*
[b] *Institut für Physik, Johannes Gutenberg-Universität Mainz, Staudinger Weg 7, 55099 Mainz, Germany*
[c] *Institut für Theoretische Physik, Freie Universität Berlin, Arnimallee 14, 14195 Berlin, Germany*
[d] *Department of Physics, Kinki University, Higashi-Osaka, 577 Japan*
[e] *Department of Physics, Nara National College of Technology, Yamatokohriyama, 639-11 Japan*

Abstract

Employing the Polyakov–Susskind approximation in a field theoretical treatment, the t–J model for strongly correlated electrons in two dimensions has recently been shown to map effectively onto an asymmetric two-dimensional classical XY model. The critical temperature at which charge–spin separation occurs in the t–J model is determined by the location of the phase transitions of this effective model. Here we report results of Monte Carlo simulations which map out the complete phase diagram in the two-dimensional parameter space and also shed some light on the critical behaviour of the transitions.

1. Introduction

The discovery of high-T_c superconductivity has inspired various new ideas and approaches in theoretical condensed matter physics. In particular, the concept of holons and spinons for systems of strongly correlated electrons provided a useful way to understand some interesting phenomena, like charge–spin separation (CSS) [1], that may happen in cuprate superconductors.

Explicitly, the so-called slave–boson or slave–fermion representation of the t–J model of electrons is often used to develop mean-field theories [2–4], which globally explain the experimentally observed phase diagram to a good extent as a first approximation. However, to calculate "higher-order" corrections to the mean-field results, one faces the fact that the system possesses a U(1) gauge symmetry, and is forced to study the dynamics of this gauge symmetry. Since the phase diagram has a region in which the gauge dynamics is realized in a strong-coupling confinement

---

* Corresponding author. E-mail: janke@miro.physik.uni-mainz.de.

phase, usual weak-coupling perturbation theory is not sufficient to estimate the above corrections.

To study this gauge dynamics in a general and non-perturbative manner, Ichinose and Matsui [5] recently developed a theory of confinement–deconfinement transition for the t–J model. There the confinement region corresponds to an electron phase where holons and spinons are confined in electrons, while the deconfinement region corresponds to CSS and holons and spinons behave as quasiparticles. The theory is based on the method of Polyakov and Susskind [6,7] for the confinement–deconfinement transition of lattice gauge theory at finite temperatures. The latter maps U(1) lattice gauge theory in $d + 1$ dimensions onto the classical XY-spin model on a d-dimensional lattice as an effective model. In Ref. [5] the same method was employed to the $(2 + 1)$-dimensional t–J model to derive an effective model which here takes the form of an *asymmetric* XY-spin model on a two-dimensional lattice. The asymmetry stems from the fact that not one but two kinds of gauge fields appear in the t–J model, reflecting that both particle–hole and particle–particle channels are relevant. As discussed in more detail in Ref. [5], the critical temperature at which CSS occurs in the t–J model is determined by the location of the phase transitions of this XY model, and the properties of the XY spins enter crucially in the analysis of the t–J model.

This motivated us to perform Monte Carlo simulations of the asymmetric XY-spin model. In this note we investigate the overall phase diagram and report finite-size scaling (FSS) analyses at four selected points along the phase transition line in the two-parameter space. The result on the phase diagram has been used in a preliminary analysis in Ref. [8] to derive a critical temperature of CSS, T_{CSS}, which indicates that the effects of gauge-field fluctuations are so large that the resulting value of T_{CSS} is only about 10% of its mean-field value. The Monte Carlo results reported below shall therefore be useful for acquiring more detailed informations on the gauge dynamics of the t–J model.

The rest of the paper is organised as follows. In Section 2 we give the definition of the effective asymmetric XY model and discuss the details of the Monte Carlo simulations. In Section 3 we present the results of our simulations, and in Section 4 we conclude with a brief summary and a few final remarks.

2. The model and simulation details

The effective model we simulated is defined by the partition function

$$Z = \left[\prod_i \int_0^{2\pi} \frac{d\theta_i}{2\pi} \right] \exp(-KE) , \tag{1}$$

with an energy

$$E = -J_1 \sum_{\langle ij \rangle} \cos(\theta_i - \theta_j) - J_2 \sum_{\langle ij \rangle} \cos(\theta_i + \theta_j) , \tag{2}$$

where i are the sites of a two-dimensional (2D) square $L \times L$ lattice with periodic boundary conditions, $\langle ij \rangle$ denote nearest-neighbour pairs, and $K = 1/k_B T$ is the inverse temperature of the asymmetric XY model system. The temperature T should not be confused with the physical temperature T_{phys} of the original t–J model which enters through the coupling constants J_1 and J_2 in Eq. (2). These parameters are known functions of T_{phys}, so that one can simply relate T and T_{phys} to discuss the physical implications for the t–J model like CSS as has been done more thoroughly in Ref. [8].

By introducing 2D unit vectors $s_i = (s_i^{(1)}, s_i^{(2)}) = (\cos(\theta_i), \sin(\theta_i))$ the energy can be rewritten as

$$E = -\sum_{\langle ij \rangle} [(J_1 + J_2) s_i^{(1)} s_j^{(1)} + (J_1 - J_2) s_i^{(2)} s_j^{(2)}] \tag{3}$$

$$= -(J_1 + J_2) \sum_{\langle ij \rangle} [s_i \cdot s_j - \eta \, s_i^{(2)} s_j^{(2)}], \tag{4}$$

where

$$\eta = 2 \frac{J_2}{J_1 + J_2} \tag{5}$$

is the asymmetry parameter. For $\eta = 0$, we obviously recover the 2D XY model which is known to undergo a Kosterlitz–Thouless (KT) phase transition at $K_c(J_1 + J_2) = 1.1199(1)$ [9]. For *any* non-zero asymmetry parameter η the O(2) symmetry of the XY model is broken to Z_2, and we theoretically expect to observe a crossover to the 2D Ising-model universality class.

The model, Eqs. (1) and (2), has symmetries under the separate reflections (i) $J_1 \to -J_1$ and (ii) $J_2 \to -J_2$. One can see this by a simple change of variables, where $\theta_i \to \theta_i + \pi/2$ for even sites and $\theta_j \to \theta_j \mp \pi/2$ for odd sites. Thus, without loss of generality, we will consider in this note only the case of ferromagnetic couplings ($J_1 \geqslant 0$, $J_2 \geqslant 0$). Furthermore, due to the reflection symmetry of the model at the line $J_1 = J_2$, we can confine ourselves to the lower triangle $J_2 \leqslant J_1$ in the 2D coupling-constant plane. We set $J_1 = 1$ except where stated otherwise explicitly. In order to get an overview of the phase diagram we have first performed for various coupling constants J_2 thermal heating and cooling cycles on relatively small lattices (24×24 and 48×48). In the thermal heating cycle we started with a completely ordered spin configuration at a low temperature (high K) and then heated the system in increments of about $\Delta K = 0.01$. The cooling cycle is defined analogously. In the Monte Carlo simulations we discretized the continuous angles as $\theta_i = 2\pi n_i/100$, $n_i = 1, \ldots, 100$. For the update we used a fully vectorized Metropolis code employing the checker-board scheme. The results for the specific heat and the magnetic susceptibility are shown in Figs. 1 and 2. The phase transition line in the KJ_1–KJ_2 plane is depicted in Fig. 3 (using the more precise U_4^*-method described in Section 3).

Having located the approximate phase transition points we next performed more elaborate FSS studies at four selected couplings: $J_2 = 0.1, 0.2, 0.4$ and 1. In each case we studied the lattice sizes $L = 24, 32, 48, 64$ and 96. Here the strategy was to perform
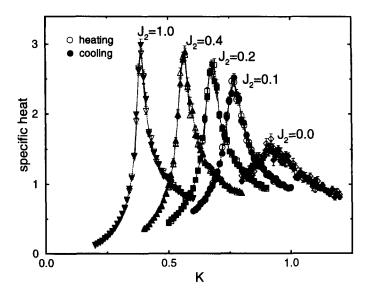
Fig. 1. Temperature dependence of the specific heat on a 24 × 24 lattice obtained in heating and cooling cycles with $J_1 = 1$. The dotted lines are only a guide to the eye and the continuous lines show the reweighting curves computed from the long runs at criticality. For comparison also data for the XY model ($J_2 = 0$) are shown.
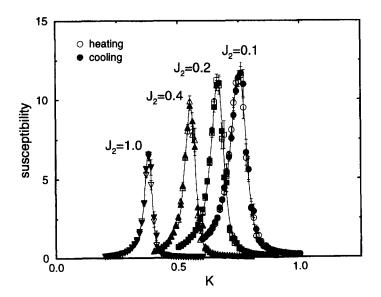

Fig. 2. Temperature dependence of the susceptibility on a 24 × 24 lattice obtained in heating and cooling cycles with $J_1 = 1$. The continuous lines are obtained by reweighting the data of the long runs at criticality.

on each lattice a single long simulation close to the pseudo-transition points defined by the maxima of the specific heat and susceptibility, and to compute the temperature dependence of the observables by reweighting techniques [10–13]. The FSS of the maxima then determines the various critical exponents. Using such FSS extrapolations
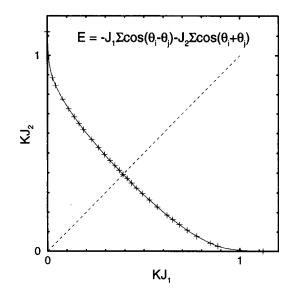
$$E = -J_1 \Sigma \cos(\theta_i - \theta_j) - J_2 \Sigma \cos(\theta_i + \theta_j)$$

Fig. 3. Phase diagram of the asymmetric 2D XY model in the KJ_1–KJ_2 plane. The dashed line is the symmetry axis. The critical behaviour of the transitions is Ising-like, except if $J_1 = 0$ or $J_2 = 0$ where the rotational symmetry is restored and the model exhibits Kosterlitz–Thouless transitions.

of the results on smaller lattices we usually obtained quite reliable a priori estimates of the simulation point K_0 on the next larger lattice. For each run we recorded the time series of the energy density $e = E/V$ and the magnetization density $m = M/V$, where $V = L \times L$ and the magnetization is defined as

$$M = \sqrt{\left[\sum_i \cos(\theta_i) \right]^2 + \left[\sum_i \sin(\theta_i) \right]^2}. \qquad (6)$$

For each lattice we performed 10 000 (20 000 for $J_2 = 1$) measurements after a sufficiently long equilibration time (between 100 000 and 500 000 sweeps). To avoid temporal correlations in the data each of these measurements was only taken after a sufficient number of sweeps through the lattice (200, 200, 200, 400 and 800 sweeps for $L = 24$, 32, 48, 64 and 96). From an analysis of the time series we confirmed that the integrated autocorrelation times τ_{int} for the energy and the magnetization are then indeed bounded by about 0.5–3.0 in units of measurements for all lattice sizes and coupling ratios (with our definition [14], $\tau_{\text{int}} = 0.5$ corresponds to completely decorrelated data). In units of sweeps the integrated autocorrelation time grows, of course quite rapidly with the system size, $\tau_{\text{int}} \propto L^z$, with a dynamical critical exponent $z \approx 2.2$. For $J_2 = 0.2$ this is illustrated in Fig. 4. As we shall see below a good scaling behaviour sets in quite early for all investigated quantities, such that for medium precision the considered lattice sizes turned out to be large enough. At any rate, in view of the rapidly increasing autocorrelations, a cluster-update algorithm (adapted to the asymmetric situation) should be used for studies of larger lattices [15].
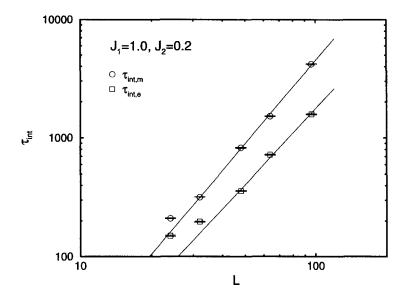
Fig. 4. Double-logarithmic plot of integrated autocorrelation times as a function of lattice size for $J_1 = 1$, $J_2 = 0.2$. Fits to $\tau_{int} \propto L^z$ yield $z \approx 2.3$ for $\tau_{int,m}$ ($L = 32, \ldots, 96$) and $z \approx 2.1$ for $\tau_{int,e}$ ($L = 48, \ldots, 96$).

To obtain results for the various observables $\mathcal{O}$ at K values in an interval around the simulation point K_0, we applied the reweighting method [10–13]. Since we recorded the time series, this amounts to computing

$$\overline{\mathcal{O}}(K) = \frac{\sum_n \mathcal{O}_n e^{-\Delta K E_n}}{\sum_n e^{-\Delta K E_n}} , \tag{7}$$

with $\Delta K = K - K_0$, and $\mathcal{O}_n$ and E_n being the measurements at the simulation point $K = K_0$ at "time" n. To obtain statistical error estimates we divided each run into 20–40 blocks and employed the standard Jackknife procedure [16,17].

From the time series it is thus straightforward to compute all energy and magnetization moments as well as all cross-correlations between these two quantities as continuous functions of temperature [18–20]. In our FSS analysis we mainly focussed on the specific heat,

$$C = K^2 V(\langle e^2 \rangle - \langle e \rangle^2) , \tag{8}$$

the susceptibility,

$$\chi = K V(\langle m^2 \rangle - \langle m \rangle^2) , \tag{9}$$

and derivatives of the magnetization with respect to inverse temperature,

$$\frac{d\langle m \rangle}{dK} = \langle m \rangle \langle E \rangle - \langle mE \rangle , \tag{10}$$

$$\frac{d \ln\langle m^p \rangle}{dK} = \langle E \rangle - \frac{\langle m^p E \rangle}{\langle m^p \rangle} , \tag{11}$$

with $p = 1$ and 2. In the infinite-volume limit all these quantities diverge at the transition point (except perhaps the specific heat). In finite systems the singularities are smeared out and replaced by maxima which scale in the critical region according to

$$C = C_{\text{reg}}(x) + L^{\alpha/\nu} f_C(x)[1 + \cdots], \tag{12}$$

$$\chi = L^{\gamma/\nu} f_\chi(x)[1 + \cdots], \tag{13}$$

$$\frac{d\langle m \rangle}{dK} = L^{(1-\beta)/\nu} f_0(x)[1 + \cdots], \tag{14}$$

$$\frac{d\ln\langle m^p \rangle}{dK} = L^{1/\nu} f_p(x)[1 + \cdots], \tag{15}$$

where C_{reg} is a regular background term, α, ν, γ, and β are the usual universal critical exponents, $f_i(x)$ are finite-size scaling functions with $x = (K - K_c)L^{1/\nu}$, and $[1 + \cdots]$ indicates correction terms which become unimportant for large enough L.

We also computed the Binder parameters [21],

$$U_{2p}(K) = 1 - \frac{1}{3} \frac{\langle m^{2p} \rangle}{\langle m^p \rangle^2}, \tag{16}$$

for $p = 1$ and 2. It is well known that the $U_{2p}(K)$ curves for different L cross around (K_c, U_{2p}^*) with slopes scaling as

$$\frac{dU_{2p}}{dK} = L^{1/\nu} f_{U_{2p}}(x)[1 + \cdots], \tag{17}$$

apart from confluent corrections explaining small systematic deviations. This allows an almost unbiased estimate of the critical coupling K_c, the universal critical exponent ν of the correlation length, and the (weakly) universal [1] renormalised charges U_{2p}^*. The slopes can be conveniently calculated as

$$\frac{dU_{2p}}{dK} = (1 - U_{2p}) \left(\langle E \rangle - 2\frac{\langle m^p E \rangle}{\langle m^p \rangle} + \frac{\langle m^{2p} E \rangle}{\langle m^{2p} \rangle} \right) \tag{18}$$

$$= (1 - U_{2p}) \left(2\frac{d\ln\langle m^p \rangle}{dK} - \frac{d\ln\langle m^{2p} \rangle}{dK} \right), \tag{19}$$

revealing in addition the close relation of Eq. (17) with Eq. (15).

3. Results

By applying reweighting techniques we first determined the maxima of C, χ, $d\langle m \rangle/dK$, $d\ln\langle m \rangle/dK$, and $d\ln\langle m^2 \rangle/dK$. The location of the maxima provided us

---

[1] Here "weakly" refers to the fact that although U_{2p}^* is insensitive to the details of the interaction and the lattice connectivity, it does depend on the boundary conditions [20] and on the shape of the lattice.

Table 1
Fitting results for the critical exponents ν, γ, and β from FSS extrapolations of some selected maxima together with various averages over *all* available data points, as well as the renormalised charges U_{2p}^* at K_c. Here Q is the goodness-of-fit parameter, and a prime denotes the derivative with respect to K

| Exp. | Obs. | $J_2 = 0.1$ | | $J_2 = 0.2$ | | $J_2 = 0.4$ | | $J_2 = 1.0$ | |
		Exponent	Q	Exponent	Q	Exponent	Q	Exponent	Q
$1/\nu$	$\ln\langle m \rangle'_{\max}$	1.030(19)	0.43	1.008(22)	0.59	1.025(55)	0.55	0.988(18)	0.29
$1/\nu$	$\ln\langle m^2 \rangle'_{\max}$	1.017(19)	0.38	1.000(21)	0.43	1.012(62)	0.54	0.995(18)	0.25
$1/\nu$	Average	1.0655		1.025		1.011		0.9813	
$1/\nu$	Weighted av.	1.0520(88)		1.014(10)		1.016(18)		0.9781(83)	
$1/\nu$	Final	1.052(19)		1.014(21)		1.016(44)		0.978(18)	
γ/ν	$\chi_{\max}$	1.798(13)	0.70	1.756(16)	0.28	1.771(15)	0.80	1.746(11)	0.65
γ/ν	Average	1.7931		1.7574		1.758		1.7528	
γ/ν	Weighted av.	1.7933(77)		1.7536(93)		1.764(10)		1.7469(65)	
γ/ν	Final	1.793(13)		1.754(16)		1.764(15)		1.747(11)	
β/ν	$\langle m \rangle$ at $\chi_{\max}$	0.1548(54)	0.47	0.1594(78)	0.49	0.142(11)	0.53	0.1331(58)	0.54
β/ν	$\langle m \rangle$ at $\langle m \rangle'_{\max}$	0.134(10)	0.11	0.145(13)	0.82	0.121(15)	0.68	0.1174(88)	0.65
β/ν	Average	0.1565		0.1626		0.1194		0.1325	
β/ν	Weighted av.	0.1511(45)		0.1572(62)		0.1318(82)		0.1292(46)	
β/ν	Final	0.1511(54)		0.1572(78)		0.132(11)		0.1292(58)	
$(1-\beta)/\nu$	$\langle m \rangle'_{\max}$	0.881(13)	0.87	0.870(20)	0.11	0.895(16)	0.06	0.855(12)	0.34
U_2^*	$U_2(K_c)$	0.64350(92)		0.6409(14)		0.6423(16)		0.64227(83)	
U_4^*	$U_4(K_c)$	0.6112(21)		0.6057(28)		0.6093(33)		0.6092(18)	

with five sequences of pseudo-transition points $K_{\max}(L)$ for which the scaling variable $x = (K_{\max}(L) - K_c)L^{1/\nu}$ should be constant. Using this information we then have several possibilities to extract the critical exponents α/ν, γ/ν, β/ν, and ν from (linear) least-square fits to the FSS Ansatz, Eqs. (12)–(15) and (17).

For the exponent ν this results altogether in 20 different estimates which are, of course, statistically not uncorrelated but differently affected by corrections to the leading FSS behaviour. With very few exceptions the fits over all data points from $L = 24$ to 96 had an acceptable chi-square value or goodness-of-fit parameter Q. As a general trend we observed that the estimates derived from the slopes of U_2 are slightly more accurate than those obtained from U_4. The most accurate numbers, however, come usually from the scaling of the maxima of the logarithmic derivatives of m. The resulting exponents $1/\nu$ are collected in Table 1, together with the arithmetic and error-weighted averages over *all* available data for $1/\nu$. Because of the neglected cross-correlations, in particular, the error estimate of the weighted average should be taken with a grain of salt. As our best values we therefore quote in the line labeled "final" quite conservatively the weighted mean and the smallest error estimate among all available fits. We see that for all four coupling-constant ratios the numerical results are consistent with the exact 2D Ising value of $\nu = 1$. For $J_2 \geqslant 0.2$ the deviations are very small and covered by the 1σ error interval. The only exception is perhaps the smallest considered asymmetry, $J_2 = 0.1$, where the final estimate is off by about 2.5σ. This may be taken as an indication that we start noticing the expected crossover to KT behaviour for $J_2 = 0$.

Table 2
Fitting results for the transition point K_c from FSS extrapolations of the various maxima locations and from the U_4^* method

Observable	$J_2 = 0.1$	$J_2 = 0.2$	$J_2 = 0.4$	$J_2 = 1.0$
C	0.77491(68)	0.68262(94)	0.56866(91)	0.39114(49)
χ	0.77474(25)	0.68309(33)	0.56819(32)	0.39102(12)
$d\langle m\rangle/dK$	0.77539(33)	0.68320(51)	0.56852(43)	0.39137(16)
$d\ln\langle m\rangle/dK$	0.77416(68)	0.68256(73)	0.5680(17)	0.39090(37)
$d\ln\langle m^2\rangle/dK$	0.77390(90)	0.68269(85)	0.5688(22)	0.39082(43)
Average	0.77462	0.68283	0.56842	0.391053
Weighted av.	0.77487(18)	0.68299(24)	0.56833(24)	0.391119(89)
Final	0.77487(25)	0.68299(33)	0.56833(32)	0.39112(12)
$U_4^*, L = 24$	0.77500(59)	0.68437(40)	0.56880(33)	0.39125(14)
$U_4^*, L = 32$	0.77463(44)	0.68397(39)	0.56875(40)	0.39158(13)
$U_4^*, L = 48$	0.77443(36)	0.68324(39)	0.56835(31)	0.39139(17)
$U_4^*, L = 64$	0.77423(31)	0.68375(28)	0.56835(21)	0.390946(89)
$U_4^*, L = 96$	0.77521(16)	0.68390(22)	0.56843(16)	0.391262(66)
Average	0.77470	0.68385	0.56854	0.391283
Weighted av.	0.77492(12)	0.68384(14)	0.56846(11)	0.391232(45)

Assuming thus $v = 1$, we have next determined estimates for K_c from the scaling of the various $K_{max}(L)$. The fitting results are compiled in Table 2 together with arithmetic and error weighted averages. Adopting the same procedure as used for the exponent v, we take as our best estimate again the weighted mean but the smallest error estimate among the five fits (which here is always that of the $K_{\chi_{max}}$ fit). This gives

$$K_c = 0.77487 \pm 0.00025 \quad (J_2 = 0.1)\,, \tag{20}$$

$$K_c = 0.68299 \pm 0.00033 \quad (J_2 = 0.2)\,, \tag{21}$$

$$K_c = 0.56833 \pm 0.00032 \quad (J_2 = 0.4)\,, \tag{22}$$

$$K_c = 0.39112 \pm 0.00012 \quad (J_2 = 1.0)\,. \tag{23}$$

A comparison of these results with the estimates from the Binder-parameter crossings shows good agreement. This can be visually inspected in Fig. 5 where $U_4(K)$ is shown for $J_2 = 0.2$.

Another quantity of interest is the asymptotic limit U_{2p}^* of the Binder parameters at K_c. For all four values of J_2 the size dependence of $U_{2p}(K_c)$ was so small that fits to the theoretically expected scaling law, $U_{2p}(K_c) = U_{2p}^* + cL^{-\omega}$, were not sensible. We rather simply took the weighted average over the five lattice sizes. For our smallest asymmetry, $J_2 = 0.1$, we obtained in this way $U_2^* = 0.64350(37)[55]$ and $U_4^* = 0.61119(76)[133]$. Here the second errors in square brackets indicate the uncertainty due to the statistical error in K_c (i.e. $\max(|U_{2p}(K_c) - U_{2p}(K_c \pm \Delta K_c)|)$). Our final estimates are shown in Table 1, where we have already combined these two types of errors. Error weighted averages over the four results for different J_2 yield
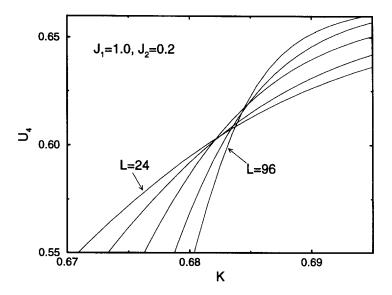
Fig. 5. The fourth-order Binder parameter $U_4(K)$ close to criticality for $J_1 = 1$, $J_2 = 0.2$.

$U_2^* = 0.64249(54)$ and $U_4^* = 0.6092(12)$. The values for U_4^* can be compared with previous MC estimates for the 2D Ising model on regular square lattices, $U_4^* = 0.615(10)$ [22] and $U_4^* = 0.611(1)$ [23], Poissonian random lattices, $U_4^* = 0.615(7)$ [24], fluctuating Regge triangulations, $U_4^* = 0.612(5)$ [19], or with an extremely precise transfer matrix computation yielding $U_4^* = 0.610\,690\,1(5)$ [25]. Since all our values for U_4^* in Table 1 are consistent with this most precise value, this gives further support that the critical behaviour of the asymmetric XY model is governed for all $J_2 \neq 0$ by the 2D Ising universality class.

For all practical purposes the estimate of U_4^* in Ref. [25] can be treated as an exact number. Assuming that the asymmetric XY model with $J_2 \neq 0$ belongs to the Ising universality class, we may now turn the argument around and reweight $U_4(K)$ in K until it hits this number at $K_{U_4} \approx K_c$, defining new pseudocritical points $K_{U_4}(L)$. Again, our accuracy does not allow to observe the theoretically expected weak size dependence of K_{U_4}. We have therefore added in Table 2 simply the values for $L = 24, 32, 48, 64$ and 96, as well as arithmetic and error-weighted averages over all five lattice sizes which here yield uncorrelated estimates. By comparing the different estimates we can conclude that the U_4^* method for locating K_c gives reliable results (with relative errors of the order of 0.1%) already for lattice sizes as small as $L = 24$. Equipped with this result it is thus quite easy to determine the complete 2D phase diagram in Fig. 3 with relatively high precision.

To extract the critical exponent ratio γ/ν we used the scaling $\chi \cong L^{\gamma/\nu} f_\chi(x)$ at the previously discussed points of constant x. The results of fits of χ_{max} as well as the averages over all fits (using the same procedure as for ν to arrive at the final estimates) can be inspected in Table 1. Except for $J_2 = 0.1$, where the final estimate is again off
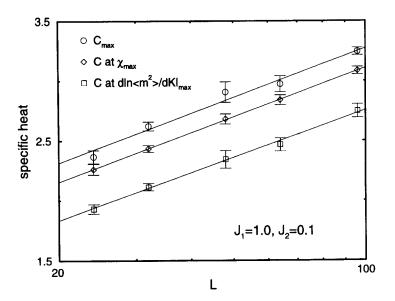
Fig. 6. Semi-logarithmic finite-size scaling plot of the specific heat at criticality for $J_1 = 1$, $J_2 = 0.1$. The straight lines are fits to $C = C_{reg} + A \ln L$ with goodness-of-fit parameters $Q = 0.46$ ($\bigcirc$), 0.997 ($\diamond$), and 0.89 ($\square$).

by about 3σ, the numerical results are fully consistent with the exact 2D Ising value $\gamma/\nu = 7/4 = 1.75$.

To extract the magnetical critical exponent ratio β/ν we used that $\langle m \rangle \cong L^{-\beta/\nu} f_m(x)$ at all constant x-values. Another method is to look at the scaling, Eq. (14) of $d\langle m \rangle / dK$ yielding $(1 - \beta)/\nu$. The fit results for β/ν and $(1 - \beta)/\nu$ are again given in Table 1. We see that all estimates for $(1 - \beta)/\nu$ are nicely consistent with the exact value of $(1 - \beta)/\nu = 7/8 = 0.875$. The exponent β/ν, however, seems to be less well determined for small values of J_2, i.e., small asymmetry, which would probably require additional simulations on larger lattices. While here also the final result for $J_2 = 0.2$ is only marginally compatible (at a 3σ-level) with the exact 2D Ising value $\beta/\nu = 1/8 = 0.125$, we obtain for $J_2 = 0.4$ and $J_2 = 1.0$ again perfect agreement.

Having found so far overwhelming evidence for the 2D Ising universality class, we expect also the specific-heat exponent α to take on the Onsager value, namely $\alpha = 0$. In this case we expect a logarithmic divergence of the form

$$C = C_{reg}(x) + A(x) \ln L + \cdots . \tag{24}$$

Indeed the data at the different fixed values of x can all be fitted nicely with this Ansatz down to the small asymmetry case $J_2 = 0.1$. This is demonstrated in Fig. 6. Clearly, our lattice sizes are much too small to discriminate between the FSS Ansatz, Eq. (24) and a power-law Ansatz with a small non-zero exponent α. This is a well-known problem with fits of the specific heat at criticality which has already been noticed before several times [19,20,24]. Overall we can conclude, however, that our data is compatible with the exact 2D Ising value of $\alpha = 0$.

4. Conclusions

We have performed a fairly detailed numerical study of the asymmetric XY model in two dimensions and obtained the phase diagram in the $KJ_1–KJ_2$ coupling-constant plane. From finite-size scaling analyses at four different coupling ratios ($J_1 = 1$; $J_2 = 0.1$, 0.2, 0.4 and 1) we find clear evidence that for $J_2 \neq 0$ the critical behaviour of the model is governed by 2D Ising Onsager exponents, as expected on theoretical grounds.

As far as the original motivation stemming from the $t–J$ model for strongly correlated electrons in two dimensions is concerned, this answers most of the questions satisfactorily. The physical implications of our results for the $t–J$ model will be discussed in a separate publication [26].

It would be interesting in its own right, however, to investigate in more detail the crossover from KT behaviour for $J_2 = 0$ to Ising behaviour for $J_2 \neq 0$ at very small coupling constants J_2. A study in this direction is under way, employing a more efficient cluster-update algorithm adapted to the asymmetric situation [15].

Acknowledgements

References

[1] P.W. Anderson, Phys. Rev. Lett. 64 (1990) 1839.
[2] G. Kotliar, J. Liu, Phys. Rev. B 38 (1988) 5142.
[3] Y. Suzumura, Y. Hasegawa, H. Fukuyama, J. Phys. Soc. Japan 57 (1988) 2768.
[4] M.U. Ubbens, P.A. Lee, Phys. Rev. B 46 (1992) 8434; B 49 (1994) 6853.
[5] I. Ichinose, T. Matsui, Nucl. Phys. B 394 (1993) 281; Phys. Rev. B 51 (1995) 11 860.
[6] A.M. Polyakov, Phys. Lett. B 72 (1978) 477.
[7] L. Susskind, Phys. Rev. D 20 (1979) 2610.
[8] I. Ichinose, T. Matsui, K. Sakakibara, preprint UT-Komaba 97-1, cond-mat/9701156.
[9] M. Hasenbusch, K. Pinn, J. Phys. A 30 (1997) 63.
[10] M. Falcioni, E. Marinari, M.L. Paciello, G. Parisi, B. Taglienti, Phys. Lett. B 108 (1982) 331.
[11] E. Marinari, Nucl. Phys. B 235 (1984) 123.
[12] G. Bhanot, S. Black, P. Carter, R. Salvador, Phys. Lett. B 183 (1987) 331.
[13] A. Ferrenberg, R.H. Swendsen, Phys. Rev. Lett. 61 (1988) 2635; 63 (1989) 1658(E).
[14] W. Janke, Monte Carlo simulations of spin systems, in: K.H. Hoffmann, M. Schreiber (Eds.), Computational Physics: Selected Methods – Simple Exercises – Serious Applications, Springer, Berlin, 1996, p. 10.
[15] C. Holm, W. Janke, T. Matsui, K. Sakakibara, work in progress.
[16] R.G. Miller, Biometrika 61 (1974) 1.
[17] B. Efron, The Jackknife, the Bootstrap and Other Resampling Plans, SIAM, Philadelphia, 1982.
[18] C. Holm, W. Janke, Phys. Lett. A 173 (1993) 8; Phys. Rev. B 48 (1993) 936; J. Phys. A 27 (1994) 2553; Phys. Rev. Lett. 78 (1997) 2265.

[19] C. Holm, W. Janke, Phys. Lett. B 335 (1994) 143.
[20] C. Holm, W. Janke, Phys. Lett. B 375 (1996) 69.
[21] K. Binder, Z. Phys. B 43 (1981) 119.
[22] K. Binder, D.P. Landau, Surf. Sci. 151 (1985) 409.
[23] D.W. Heermann, A.N. Burkitt, Physica A 162 (1990) 210.
[24] W. Janke, M. Katoot, R. Villanova, Phys. Lett. B 315 (1993) 412; Phys. Rev. B 49 (1994) 9644.
[25] G. Kamieniarz, H.W.J. Blöte, J. Phys. A 26 (1993) 201.
[26] C. Holm, W. Janke, T. Matsui, K. Sakakibara, in preparation.